Effects of Iron Oxide Nanoparticles as T_2-MRI Contrast Agents on Reproductive System in Male Mice

Heyu Yang
First Affiliated Hospital of Anhui Medical University
Hui Wang
First Affiliated Hospital of Anhui Medical University
Chenghao Wen
First Affiliated Hospital of Anhui Medical University
Shun Bai
first affliated hospital of university of science and technology of China
Pengfei Wei
binzhou medical university
Bo Xu
First Affiliated Hospital of Science and technology of China University
Yunjun Xu
University of Science and Technology of China
Chaozhao Liang
First Affiliated Hospital of Anhui Medical University
Yunjiao Zhang
South China University of Technology
Guilong Zhang
binzhou medical university
Huiqin Wen
First Affiliated Hospital of Anhui Medical University
Li Zhang (lzhang@ahmu.edu.cn)
First Affiliated Hospital of Anhui Medical University

Research Article

Keywords: Magnetic resonance imaging, Contrast agents, Iron oxide nanoparticles, Reversible toxicities, Reproductive system

Posted Date: October 20th, 2021

DOI: https://doi.org/10.21203/rs.3.rs-965062/v1

Version of Record: A version of this preprint was published at Journal of Nanobiotechnology on March 2nd, 2022. See the published version at https://doi.org/10.1186/s12951-022-01291-2.

Abstract

Iron oxide nanoparticles (IONPs)-based contrast agents are widely used for T_2-weighted magnetic resonance imaging (MRI) in clinical diagnosis, highlighting the necessity and importance to evaluate their potential systematic toxicities. Although a few previous studies have documented the toxicity concerns of IONPs to major organs, limited data are available on the potential reproductive toxicity caused by IONPs, especially when administrated via intravenous injection to mimic clinical use of MRI contrast agents. Our study aimed to determine whether exposure to IONPs would affect male reproductive system and cause other related health concerns in ICR mice. The mice were intravenously injected with different concentrations IONPs once followed by routine toxicity tests of major organs and a series of reproductive function-related analyses at different time points. As a result, most of the contrast agents were captured by reticuloendothelial system (RES) organs such as liver and spleen, while IONPs have not presented adverse effects on the normal function of these major organs. In contrast, although IONPs were not able to enter testis through the blood testicular barrier (BTB), and they have not impaired the normal testicular structure or altered the serum sex hormones levels, IONPs exposure could damage Sertoli cells in BTB at a relative high concentration. Moreover, IONPs administration led to a short-term reduction in the quantity and quality of sperms in a dose-dependent manner, which might be attributed to the increase of oxidative stress in epididymis. However, the semen parameters have gradually returned to the normal range within 14 days after the initial injection of IONPs. Collectively, these results demonstrated that IONPs could cause reversible damage to the reproductive system of male mice without affecting the main organs, providing new guidance for the clinical application of IONPs as T_2-MRI contrast agents.

Introduction

Accurate and sensitive imaging examinations are of great importance to timely diagnosis and effective treatment of diseases. By possessing deep-tissue penetration, high spatial resolution with soft-tissue sensitivity, no radiation and several other unique advantages, magnetic resonance imaging (MRI) has been widely used in clinical practice [1, 2]. Compared with ultrasound, computerized tomography (CT), MRI plays an irreplaceable role in the diagnosis of cardiovascular diseases [3, 4], neurosurgical and neurological diseases [5, 6], arthritis and various types of tumors [7–9]. Although MRI has multiple scan sequences and parameters, such as T_1/T_2-weighted imaging (T_1/T_2-WI), diffusion-weighted imaging (DWI), dynamic contrast-enhanced imaging (DCEI) and magnetic resonance spectroscopic imaging (MRSI), it sometimes can not distinguish specific tumor tissues clearly due to the similar signal intensities of tumor tissues with adjacent normal tissues. Therefore, DCEI with intravenously-injected contrast agents to achieve signal difference amplification has gradually become a routine approach in clinical MRI diagnosis and prognosis evaluation [10, 11].

Superparamagnetic iron oxide nanoparticles (SPIONs) are currently the most successfully used nano-sized contrast agents for T_2-WI and DCEI in MRI diagnosis [12, 13]. In spite of the growing variety of SPION formulations approved by the Food and Drug Administration (FDA) for use in humans as iron-

deficiency therapeutics or as MRI contrast agents, e.g., Feridex®, Umirem® and Resovist® [14–16], constant reevaluation of the theranostic efficacy as well as the potential risk of side effects led to a changing area of their application in most cases. Therefore, the discovery of hidden side effects can bring enlightenment to clinical practice and guide the correct and reasonable use of contrast agents. On the basis of the present knowledge, these new-generation nanomaterial-based MRI contrast agents are primarily used for diagnostic applications in tumorous diseases, while they sometimes are also employed to diagnose benign diseases such as strain of joints. Accordingly, more close attention should be paid to their potential short- and long-term toxicities for avoiding harmful side effects in clinical diagnostics.

Nano-sized iron oxide contrast agents are generally regarded as biocompatible materials. Concretely, a parallel comparative *in vivo* mouse model study among extremely small iron oxide nanoparticles (ESIONs), manganese oxide nanoparticles (MnO NPs) and clinically used gadolinium-based contrast agents (GBCAs) has documented a better biosafety profile possessed by ESIONs than that of MnO NPs and GBCAs [17]. The follow-up study further revealed that compared with GBCAs, ~8 nm iron oxide nanoclusters (IONCs) exhibited a favorable biocompatibility and much lower risk of nephrogenic systemic fibrosis, suggesting the possibility of substituting GBCAs with IONCs in clinical MRI diagnosis for those patients with impaired renal function [18]. Similarly, no significant toxicity concerns of dimercaptosuccinic acid (DMSA)-coated IONPs have been raised in a nonhuman primate model during the 120-day period, although DMSA-coated IONPs may show preferential accumulation in lung and brain tissues [19]. In addition to the intravenous injection of IONPs, the uptake, distribution and toxicity profile has also been evaluated in a rat model by intestinal perfusion of ultrasmall (4 nm core) iron oxide nanoparticles (USIONs) coated with tartaric/adipic acid. As a result, the *in vivo* absorption through the small intestine reached above 79% of the initial perfusion of USIONs, however, the intact particles around the intestinal microvilli have not caused significant tissue damage. Moreover, such high absorption levels have not compromised cell viability, demonstrated by cytotoxicity, reactive oxygen species (ROS) production, genotoxicity and lipid peroxidation assays in Caco-2 and HT-29 enterocytes-like models [20].

Notably, as male reproductive system has been regarded as vulnerable and even more sensitive to exogenous materials than other organ systems, in addition to the aforementioned systematic assessment of the functional damage of major organs like heart, liver, spleen, lung, kidney and hematopoietic system, potential side effects on male reproductive system had also been evaluated for a few types of materials. For one thing, some nanomaterials could pose an unfavorable effect on the male reproductive system via altering spermatogenesis and causing histopathological damage [21]. Among them, PbSe NPs were able to accumulate in the testis, followed by decrease in testis and epididymis coefficients, disorder of sex hormones, destruction of normal seminiferous tubule structures, reduction in both quantity and quality of sperms, further leading to an impaired fertility [22]. Similarly, repeated intravenous injections of Mn_3O_4 nanoparticles into male mice could cause particles accumulation in the testis, then triggered oxidative stress reflected by malondialdehyde (MDA) upregulation, disturbed the balance among sex hormones and finally displayed decreased fertility [23]. However, for another, several nanoparticles are free of harmfulness to the male reproductive system. For instance, different

modifications of gold nanoparticles could accumulate in the testis of male mice, and even pass through the BTB to enter germ cells, while they have not presented any obviously adverse effect on normal fertility [24].

Intriguingly, nanomaterials with same component may have distinct or even opposite effects on male reproductive system under different conditions. For instance, many studies have reported the histological damage in testicular and epididymal tissues after exposure to zinc oxide nanoparticles (ZnO NPs) *in vivo*, including multinucleated giant cells formation, germ cell layers disorganization and immature germ cells detachment [25, 26]. However, given the biological activities in activating steroidogenic enzymes and alleviating oxidative stress, ZnO NPs supplementation could also minimize the adverse effects on the sperm parameters, histological structure of the testis and epididymis, which were commonly observed after nicotine exposure in male rats [27]. In other words, nanomaterials may have a negative or positive effect on male reproductive system, and it is not possible to deduce their potential reproductive toxicity.

With the widespread use of contrast agents in clinical practice, a considerable number of male patients within reproductive ages have necessarily received MRI examinations with intravenously injected contrast agents. Therefore, for these populations, the risk assessment of the reproductive function should be carefully conducted. Especially, the concrete profile of the reproductive system exposed to intravenously injected IONPs, such as the distribution of IONPs in reproductive organs, their ability to pass through reproduction-relevant physiological barriers and the effects on sperm parameters or sex hormones, are still largely unknown.

In this study, we have successfully designed the poly (acrylic acid) (PAA)-capped IONPs, and investigated their biodistribution, major organs toxicities, especially reproductive toxicities, which provided an important reference for use of IONPs as T_2-MRI contrast agents. To mimic the clinical applications in terms of dosage, duration of treatment and route of administration, we intravenously injected different concentrations of IONPs via the tail vein into adult male ICR mice. Our results showed that IONPs had negligible toxicity in major organs such as heart, liver, spleen, lung and kidney, which was consistent with previous reports [14–19]. However, we found the accumulation of IONPs in epididymis, and IONPs were toxic to the reproductive system including testis and epididymis during short-term, resulting in impaired sperm quantity/quality and even apoptotic sperms (Fig. 1). Nevertheless, the sperm count and quality returned to the normal range after 2 weeks since initial injection of IONPs. These findings will provide a valuable enlightenment that the use of IONPs may lead to temporary but reversible impaired fertility, suggesting male patients who received MRI examinations with IONPs as T_2-MRI contrast agents may need to delay fertilized behavior during a certain period.

Materials And Methods

Materials

$FeCl_3 \cdot 6H_2O$ (98%), oleic acid (OA, 90%), 1-octadecene (ODE, 90%) and poly (acrylic acid) (PAA, Mw=1800) were purchased from Sigma Chemical Ltd; sodium oleate (95%) was purchased from TCI Company; normal hexane, chloroform, ethanol, dimethyl sulfoxide were purchased from the Shanghai Reagent Company (P. R. China). All chemicals were analytical and used as received without further purification. Alanine aminotransferase (ALT) (C009-2-1), Aspartate aminotransferase (AST) (C010-2-1), Creatinine (Cr) (C011-2-1) and Blood urea nitrogen (BUN) (C013-2-1) Assay kit were obtained from NJJCBIO (Nanjing, China). Follicle-stimulating Hormone (FSH) (JYM0417Mo), Luteinizing Hormone (LH) (JYM0341Mo) and Testosterone (T) (JYM0373Mo) Elisa kit were purchased from Wuhan jiyinmei Biotechnology Co., Ltd (Wuhan, China). Automatic Sperm Analyzer (ML-MD06200B) and Sperm Counting Chamber (ML-CASA60-4) were purchased from Nanning Song Jing Tianlun Bio-technology Co., Ltd (Nanning, China).

Synthesis of Iron Oxide Nanoparticles and Surface Modification

Monodisperse ultrasmall iron oxide nanoparticles were synthesized via a modified protocol [28]. The as-prepared iron oxide nanoparticles were redissolved into chloroform to achieve a stock solution (5 mg (Fe) /mL). 2 mL stock solution was mixed with PAA in 200 mL dimethyl sulfoxide (DMSO) by sonication. The molar ratio of the exchange ligand to Fe atoms was set roughly at 5 to 1 [29]. After 48 h, the hydrophilic PAA-capped iron oxide nanoparticles were collected by centrifugation. Then, the water-soluble nanoparticles were washed by deionized water, followed by redispersion into water.

MR Performance Investigation and MR Phantom Analysis

MR investigation on 3.0 T was carried out on Siemens 3.0 Tesla MR scanner. T_2 weighted MR images were acquired using Turbo Spin Echo (TSE) sequence with a knee coil. Imaging parameters for T_2 MR imaging were as follows: repetition time (TR): 5000 ms, echo time (TE): 40, 103, 206 ms, FOV: 240 × 240 mm.

Characterization

The phase of the as-prepared product was characterized by X-ray power diffraction (XRD) analyses; which was carried out on a Philips X'Pert PRO SUPER X-ray diffractometer equipped with graphite monochromatized Cu Ka radiation and the operation voltage and current were maintained at 40 kV and 40 mA; respectively. Transmission electron microscopy (TEM) was investigated by Hitachi 7700. The magnetic properties of the samples were measured by a superconducting quantum interface device (SQUID) magnetometer (Quantum Design MPMS XL). Particle size and zeta potential were examined by Malvern Zeta analyzer (ZS-90 nanosizer, Malvern Instrument, UK). FT-IR spectra were measured using a FT-IR spectrometer (Thermo Nicolet 8700). All the concentrations of our products were measured by inductive coupled plasma atomic emission spectrometer (ICP-AES) (Thermo Fisher iCAP 7400).

Animal Models

The male ICR mice (5 - 6 weeks old, approximately 20 g body weight) were purchased from the Animal Experiment Center of Nanjing University (Nanjing, China), and housed in an isolated animal room with

water and rodent food supplements. The animals were acclimated to the environment for 1 week prior to the experiments. All animal experimental protocols and procedures were reviewed and approved by the Institutional Animal Care and Use Committees on Animal Care of Anhui Medical University (Approval No. LLSC20211064).

In *vivo* Biocompatibility Assay

For *in vivo* biocompatibility evaluation of IONPs, ICR mice were injected with different concentrations of IONPs solution via tail vein (100 μL, 2.5 mg/kg, 10mg/kg and 20 mg/kg), and PBS was injected as a control. At predetermined time points, the mice were sacrificed, and the organs were harvested, including the brain, heart, liver, spleen, lung, kidney, testis and epididymis. The amounts of Fe ions in various organs were quantitatively determined by ICP-AES.

In *vivo* Safety Evaluation

To investigate the toxic profiles of IONPs, the ICR mice were divided into four groups that were intravenously administered PBS and IONPs at dosages of 2.5 mg/kg, 10 mg/kg and 20 mg/kg, respectively. Body weights were measured after intravenous administration until day 28. After 1, 3, 7, 14 and 28 days, the mice were sacrificed, and the organs were harvested for H&E staining. To further evaluate the safety in *vivo*, the serum levels of urea nitrogen (BUN), serum creatinine (CRE), alanine aminotransferase (ALT) and aspartate transaminase (AST) were analyzed using ELISA kits (Catalog number: C013-2-1, C011-2-1, C009-2-1, C010-2-1, respectively, Nanjing Jiancheng Bioengineering Institute, Jiangsu, China).

Sperm Parameters Analysis

To evaluate the toxicity of IONPs to sperms, the ICR mice were intravenously administered PBS and IONPs at dosages of 2.5 mg/kg, 10 mg/kg and 20 mg/kg, respectively. These mice were closely monitored for 1, 3, 7, 14 and 28 days after the initial drug exposure. Then, the left cauda epididymis was removed and immediately put into 50 mL of preheated DMEM medium at 37°C. Afterwards, it was cut into small pieces and incubated at a constant temperature of 37°C for 30 min to let the sperms release to the medium sufficiently. The sperms suspension was analyzed by a computer-aided semen analysis system (ML-MD06200B), Nanning Song Jing Tianlun Bio-technology Co., Ltd.) for the sperm comprehensive evaluation, including the concentration, mobility, vitality, and sperm motion parameters.

In *vivo* Toxicity Evaluation of Testis

To investigate the toxicity of IONPs to testis, the ICR mice were intravenously administered PBS and IONPs at dosages of 2.5 mg/kg, 10 mg/kg and 20 mg/kg, respectively. After the initial drug exposure at 1, 3, 7, 14 and 28 days, the mice were sacrificed, and the testis was harvested. The testis image was

recorded and testis index (testis weight/body weight, w/w %) was calculated after intravenous administration. Then, the H&E staining was used to evaluated the damage of testis caused by IONPs, and the amounts of Fe ions in testis were quantitatively determined by ICP. In addition, the serum of mice was collected to measure the sex hormones including follicle-stimulating hormone (FSH), testosterone (T) and luteinizing hormone (LH) by the ELISA kit from Cusabio (Wuhan, China).

In *vivo* Toxicity Evaluation of Epididymis

To know the toxicity of IONPs to epididymis, the ICR mice were intravenously administered PBS and IONPs at dosages of 2.5 mg/kg, 10 mg/kg and 20 mg/kg, respectively. After the initial drug exposure at 1, 3, 7, 14 and 28 days, the mice were sacrificed, and the epididymis was harvested. The epididymis index (epididymis weight/body weight, w/w %) was calculated after intravenous administration. Then the amounts of Fe ions in epididymis were quantitatively determined by ICP-AES, and the H&E staining and TUNEL staining (Catalog number: C1089, Beyotime, Jiangsu, China Roche, Mannheim, Germany) were used to evaluated the damage of epididymis caused by IONPs. Images were captured with a fluorescence microscope (Olympus BX61W1with Fluoview FV1000 software, Japan), and then analyzed using the ImagePro software. In addition, the right epididymis tissue homogenates were prepared to measure the epididymal malondialdehyde (MDA) and total superoxide dismutase (T-SOD) following the commercial kit's protocol (Jiancheng Biotech, Nanjing, China).

Statistical Analysis

All results were expressed as the means ± standard error of mean (SEM) as indicated. Student's t test was used for the comparison of differences between two groups, while one-way analysis of variance (ANOVA) was applied to evaluate the statistically significant differences among multiple groups. All statistical analyses were performed using SPSS 19.0 (SPSS Inc., Chicago, IL). The threshold for statistical significance was $P < 0.05$.

Results And Discussion

Preparation of Hydrophilic Iron Oxide Nanoparticles

It is well-established that surface modifications of IONPs could not only effectively enhance the stability of nanoparticles but also potentially affect the biocompatibility and pharmacokinetics of nanoparticles *in vivo* [30]. Some studies have found that positively-charged IONPs possessed a higher affinity to attach to the cell membranes, and they were more likely to be internalized in much larger amounts compared with negatively-charged IONPs [31]. Moreover, greater bioaccumulation, more protein adsorption and significant toxicity were also observed in positively-charged IONPs [31, 32]. Hypersensitivity reaction reported in most iron-based agents has recently attracted close attention [33, 34]. Attractively, lower probability of hypersensitivity was benefited from the high carboxyl group coating density of negatively-charged IONPs [35]. According to the aforementioned discoveries, a kind of low molecular weight poly

(acrylic acid) (PAA) was selected to decorate and manufacture the monodisperse ultrasmall iron oxide nanoparticles via a modified protocol. The as-prepared 6 nm-diameter oleic acid-capped iron oxide nanoparticles initially dispersed in chloroform (Additional file 1: Fig. S1) [28]. After ligand exchange on nanoparticle surfaces by PAA, the hydrophilic PAA-capped iron oxide nanoparticles (IONPs) were obtained [29]. IONPs dispersed into aqueous solution were then examined by transmission electron microscopy (TEM) and dynamic light scattering (DLS) to demonstrate uniformity of size and distribution. TEM revealed the particle size of IONPs was ~6 nm (Fig. 2a), and the hydrodynamic diameter in aqueous solution measured by DLS was 8.62 ± 2.18 nm (Fig. 1b), validating its excellent monodispersion and stability. The overall zeta potential of IONPs (-22 mV) was measured using zeta seizer, indicating successful surface functionalization of the as-prepared hydrophilic nanoparticles. The FT-IR spectra further confirmed the surface modification of IONPs by PAA (Additional file 2: Fig. S2). The adsorption bands at 2923 and 2853 cm^{-1} were attributed to the -CH_2- groups [36]. The peak at 1718 cm^{-1} was assigned to the carbonyl group (C=O) [29]. The appearance of two peaks at 3440 and 1631 cm^{-1} were ascribed to the -OH bending vibration, which was consistent with previously reported PAA-coated iron oxide nanoparticles [29, 36, 37]. The X-ray diffraction (XRD) pattern of IONPs was illustrated in Fig. 2c, which corresponded to magnetite (JCPDS 19-0629). IONPs dispersed in aqueous solution could form a stable suspension, and it showed a good response to the magnet (inset of Fig. 2d). A SQUID test was carried out to investigate the magnetic property of the acquired IONPs. As shown in Fig. 2d, IONPs had a saturation magnetization (Ms) of 65.95 emu/g Fe at room temperature.

Relaxometric Property of IONPs

To ascertain the MRI relaxation property of IONPs, the transverse relaxation time of IONPs with different Fe concentrations was measured by a clinical 3.0 T MRI scanner. An enhancement in the T_2-weighted MR signals was observed as the concentration of IONPs increased (from 0.02 to 0.08 mM of Fe), leading to a raise in the signal of the corresponding MR images (Fig. 2e). The corresponding transverse relaxivity (r_2) of IONPs was calculated to be 231.49 $mM^{-1}s^{-1}$, indicating a good MR imaging behavior (Fig. 2f).

Investigation of the Biocompatibility of IONPs *in vivo*

Intravenous injection is the most routinely used approach for administration of IONPs as MRI contrast agents, and intravenously injected IONPs could also circulate through the bloodstream to multiple organs. In general, IONPs are selectively taken up by the liver and spleen [17, 18, 38], while a few reports also documented the retention or elimination of IONPs in the lung or kidney [39, 40], subsequently raising the toxic concerns in major organs. As IONPs were injected intravenously, the hemolysis rate of IONPs was firstly evaluated, and the rate was calculated to be almost zero, indicating the excellent haemocompatibility of IONPs and promising intravenous administration approach (Additional file 3: Fig. S3). Secondly, the potential toxicity of IONPs to major organs has been evaluated. Body weight (BW) is one of the simple, intuitive and effective indexes to reflect systemic toxicity, as shown in Fig. 3a, compared with the PBS group, there was no BW loss in the IONPs group treated with different doses. The

BW of mice injected with high dose of IONPs (26.97 ± 0.34 g) on the first day were equivalent to the control group (26.87 ± 0.43 g), and on the 28th day, the BW of mice administrated with high-dose IONPs (38.57 ± 1.22 g) were even slightly heavier than the control group (36.29 ± 0.54 g), which exhibited their negligible systemic toxicity *in vivo*. To lend more direct evidence regarding IONPs on specific major organs, the accumulation profile of IONPs in heart, liver, spleen, lung, kidney and brain was depicted inductively coupled plasma atomic emission spectrometer (ICP-AES) on 1, 3 and 7 days after intravenous injection of IONPs. As a result, the average amounts of Fe ions retained in organs were 22.63 % ID/g (liver), 8.98 % ID/g (spleen), 8.22 % ID/g (lung), 3.92 % ID/g (heart), 1.63 % ID/g (kidney) and 0.56% ID/g (brain) in descending order 24 h after initial injection (Fig. 3b). Obviously, IONPs were mainly accumulated in liver, spleen and lung, while negligible amounts were distributed in brain, which process may be hampered by blood-brain barrier (BBB). With the increase of time, the concentration of Fe ions in the tissues decreased rapidly. For example, the amount of Fe ions in liver reduced from 22.63 % ID/g of the first day to 4.07 % ID/g of the seventh day, and the decrease trend was also observed in the other organs. Later on, the histopathological examination (hematoxylin-eosin staining, H&E staining) was utilized to support the biosafety profile of IONPs in major organs (Fig. 3c and Additional file 4-7: Fig. S4-7), in which no abnormal changes in the pathological cellular structures or hyperemia, edema, cell death and other obvious injuries were observed, indicating no significant risk of the IONPs to ICR mice following intravenous injection. In details, normal lung parenchyma was observed, and the alveoli presented a vacuolated thin-walled structure. In the hepatic tissues, hepatocytes arranged in radial lines around the central vein. Meantime, the red pulp and follicles of the white pulp were well organized, indicating physicological spleen tissues. For the kidney, the mesangium appeared normal without obvious damage and the glomerular capillary or Bowman's capsule was observed in a typical nephron. Lastly, the myocardium structure was complete and myocardial cell morphology was normal. In addition, the most important serum biochemical parameters, including blood urine nitrogen (BUN), creatinine (CRE), aspartate aminotransferase (AST) and alanine aminotransferase (ALT), were used to present the function of main organs after IONPs administration (Fig. 3d-g). The results showed that these laboratory parameters in IONPs-treated mice with doses from 2.5 mg/kg to 20 mg/kg at each timepoints (up to the 28th day) were within the normal range, in other words, they have not significantly altered compared with the control group. In addition, there were no significant differences among each groups treated with low-, middle- and high-dose IONPs, respectively. For instance, no obvious increase in ALT value was documented on the first day from low-dose group (17.18 ± 2.17 U/L) to medium-dose group (17.58 ± 1.31 U/L) or high-dose group (16.29 ± 2.07 U/L). Collectively, all the above results indicated that there were no obvious toxicities to major organs of IONPs, which was in consistent with the previous reports regarding systematic toxicity evaluation of IONPs [6–8].

Evaluation of the Sperm Quantity and Quality *in vivo*

Reproductive diseases have raised growing concerns worldwide and the male factor accounts for a considerable proportion of the problems. Sperm cell is responsible for carrying the paternal genetic complement to the oocyte and forming an euploid zygote, which holds great importance to maintain

normal fertility [41]. However, compared with somatic cells, spermatozoa are relatively vulnerable to oxidative stress, external stimuli and many other factors, owing to their limited capability of antioxidant protection and DNA repair mechanisms [42]. Therefore, the impact of IONPs on male reproductive system needs to be carefully evaluated, in addition to the systematic toxicity assessment of the aforementioned major organs. Accordingly, the semen analysis profiles on male ICR mice intravenously (i.v.) injected with IONPs at low-, middle- or high-dose (2.5 mg/kg, 10 mg/kg and 20 mg/kg, respectively) were closely monitored for 28 days. As a result, the amount of normal sperm in the epididymis significantly reduced in a dose-dependent manner. On the first day after injection, the number of sperm dropped precipitously, we could only observe the presence of a small amount of sperm (approximately 21.7 % of the normal value) in low-dose group and even hardly counted the sperm (less than 8 % of the normal value) in high-dose group (Fig. 4a). This dose-dependent reduction of sperm quantities also appeared on the 3rd and 7th days after initial injection, although the sperm counts have gradually increased, as compared with the first day post-injection. For instance, the sperm counts in epididymal tissue suspensions were approximately 7.1 %, 14.4 % and 25.6 % of the normal value on the first, third, and seventh day after high-dose injection, respectively (Fig. 4b). Notably, the sperm quantity has returned to the physiological range on the 14th day, and kept normal until the observed duration of 28 days (Fig. 4a, b). As for male reproductive function, sperm quality possesses equal or even more importance than sperm quantity [43]. Thus, sperm qualities including viability and motility were evaluated following IONPs injection. Consequently, in consistent with the alternation in sperm quantities, IONPs impaired sperm qualities in a dose-dependent manner at each checkpoints of the first, third, seventh day post-treatment, and the harmful effect achieved the peak on the first day after low-, middle- or high-dose injection. Concretely, on the first day after injection of IONPs, the sperm viability rate of the low-dose group (28.56 ± 1.14 %) was significantly lower than that of the control group (49.79 ± 0.57 %), let alone the middle-dose group (17.56 ± 0.81 %) or the high-dose group (8.75 ± 0.32 %) (Fig. 4c). At the meantime, sperm motility showed almost identical changing pattern with sperm viability, no matter which doses of IONPs were administrated in each timepoints. For instance, the motility rate was extremely lower in the high-dose group (2.74 ± 0.38 %), compared to that in the control normal group (39.43 ± 0.77 %) (Fig. 4d). Notably, in accordance with that the sperm counts gradually increased and returned to the normal range on the 14th day, the sperm viability and motility also recovered to the normal range in the same duration, suggesting that the toxicities of IONPs to sperm quantity and quality were temporary and could be reversible within 2 weeks. In consideration that the sperm were released from the epididymal fragment to the buffer followed by measurement [44], sperm with normal viability and motility in the control group could almost entirely release from the epididymis into the buffer, while in IONPs-injected groups, the total counted number of sperm might be lower than it actually was, demonstrating the proportion of functional sperms should be further lower than currently estimated. Collectively, these findings raised an important clinical implication that there would be a temporary but recoverable loss of sperm quantity and quality after intravenous injection of IONPs. If a male patient has received MRI examination with IONPs as contrast agents, the fertilized behavior should be delayed until the semen parameters are recovered, which may need some duration.

Evaluation of Hormones and Testicular Indexes after IONPs Accumulation

Sperms are produced in seminiferous tubules of the testis, followed by being transported and stored in the epididymis for leaving the male body (Fig. 4e). Therefore, the damage to testis or/and epididymis may be potential causes of the decline of sperm quantity and quality after injection with IONPs. Normal testicular function, being dependent upon hormones acting through endocrine or paracrine manners, is essential for germ cell homeostasis *in vivo* [45]. Among these hormones, follicle-stimulating hormone (FSH), luteinizing hormone (LH) and testosterone (T) are particularly important to male germ cell fate, as the disorder of them would induce aberrant sperm parameters and even germ cell apoptosis [46]. To explore whether the reduction of sperm quantity and quality was associated with the abnormal levels of hormones in the mice injected with IONPs, we measured FSH, LH and testosterone, respectively. The results revealed the three hormones in mice treated with IONPs fluctuated within the normal ranges (Fig. 5a-c). Specifically, the levels of FSH (29.99 ± 0.99 ng/mL) and LH (5.93 ± 0.08 pg/mL) in mice treated with 20 mg/kg IONPs at the first day were almost equivalent to the control group (31.40 ± 0.53 ng/mL and 5.87 ± 0.04 pg/mL). In addition to these two hormones that secreted by pituitary gland, testosterone also presented the negligible alternation between the IONPs-injected group (2045.09 ± 13.14 pg/mL) and the control group (2084.35 ± 14.48 pg/mL) at the first day. Therefore, the normal hormone levels indicated that the damage to the testis of IONPs was extremely limited or even absent. Later on, to further explore the cause of the sperm loss and disability, we observed the testicular size, weight and shape in each groups. The results showed that there were no significant changes in testicular size and shape of the mice injected with IONPs with the comparable control group (Fig. 5d). Concretely, testicular weight increased from 105.80 ± 2.15 mg of the first day to 142.20 ± 2.87 mg of the 28th day after 20 mg/kg IONPs injection, which tendency was also observed in the other groups (Additional file 8: Fig. S8). To exclude the effect of age on testicular weight and more intuitively understand testicular changes, testicular index was introduced to further evaluation, which also verified the negligible differences among each groups (Fig. 5e), indicating that the macro-damage of IONPs to the testis was ignorable.

Unlike most other organs, testis possesses a unique structure called blood-testis barrier (BTB) that is composed of connective tissue, capillary endothelium, basal membrane of spermatogenic epithelium and Sertoli cell tight junction, which could not only preventing sperm antigens from escaping outside the spermatogenic tubules but also avoiding harmful substances from entering the testis to maintain environmental homeostasis for sperm development [47]. Therefore, to identify whether IONPs could enter and accumulate in the testis, ICP-AES was used to detect the abundance of Fe ions. Compared with the control group, there was no additional accumulation of Fe ions in the testis of mice injected with IONPs at each timepoints (Fig. 5f). Even at the first day after injection of IONPs that the sperm quantity and quality decreased most obviously, the concentration of Fe ions in the control group (32.75 ± 0.71 μg/g) was not significantly higher than that in the low-, middle-, high-dose groups administrated with IONPs (31.60 ± 2.20 μg/g, 29.73 ± 1.20 μg/g and 32.86 ± 1.26 μg/g, respectively). These results confirmed that IONPs have not entered into the testis.

Observation of the Histological Changes in Testis after IONPs Accumulation

The index to reflect the spermiogenesis is an important reference for judging testicular tissue injury, but not the only criterion. In addition to the detection of the objective laboratory indicators, slight injury which may cause the subtle changes of the testis, should also be carefully assessed. Accordingly, the H&E staining was used to display the structures of the testis. As a result, the structures have not shown significant differences between the control group with low- and middle-dose IONPs injection groups, while a few scattered abnormal cells were observed in the testis of mice with high-dose injection of IONPs on the first day (Fig. 5g), suggesting high-dose IONPs might cause the apoptotic cell death in testis. Johnsen score is routinely used for histologically grading in testis H&E staining, which is an effective and quantitative method to evaluate histological features and morphological changes to various pathological factors affecting testicular cells, mostly when there is no immediate or only minimal clinical alteration [48]. In this study, we used the standard Johnsen scoring system to evaluate the pathological changes of testis. As shown in Additional file 9: Fig. S9, at the first day after injection with low- and middle-dose IONPs, the Johnsen scores of the testis were both 9.67 ± 0.21, almost the same with that of the control group, while after the high-dose IONPs injection (20 mg/kg), the Johnsen score of the testis (9.17 ± 0.31) was significantly lower than the control group (9.83 ± 0.17), suggesting slightly impaired spermatogenesis, which was characterized by increased late spermatids and disorganized epithelium in testis [48]. Consistent with the observation of sperm parameters and other indicators, the most severe damage occurred at the first day after IONPs injection and gradually recovered within 2 weeks (Additional file 9: Fig. S9). However, as the presence of BTB prevented the entry of IONPs into the testis, it was quite interesting to explore why did the apoptotic cells appear after high-dose IONPs injection. In testis, there is a population of cells named Sertoli cell, which has receptors for the hormonal regulators of spermatogenesis such as FSH and testosterone, and also provides paracrine factors, nutrients, cytokines and biologically active peptides that essential for supporting spermatogenesis and fertility [49]. Notably, BTB is created by adjacent Sertoli cells near the basement membrane to divide the seminiferous epithelium into the basal and adluminal (apical) compartments, and subsequently serves for successful postmeiotic spermatid development in the apical compartment [50]. Sertoli cells on the front lines might be damaged by those toxic substances and lead to functional impairment or even cell death in the testis. As no morphological abnormalities in the Sertoli cells were observed from H&E staining of testis, we hypothesized that the extremely low-amount IONPs have entered into the Sertoli cells and impaired their function, consequently leading to the apoptosis of a few spermatogonia. To verify this hypothesis, we have detected the markers near the basal membrane to evaluate the function of Sertoli cells. Among these markers, Occludin is a tight junction protein, which participates in forming the paracellular barrier that mediates the communications of substances in the intercellular compartments between Sertoli cells [51], and N-cadherin is responsible for cell adhesion and recognition [52]. The immunohistochemical (IHC) images revealed that IONPs injection decreased the local expression and density of the markers (Fig. 5h, i). In addition, the tight junction supported by Occludin became discontinuous, which further indicated that the function of the Sertoli cells was partially impaired (Fig. 5i). Collectively, Sertoli cells

internalized a tiny amount of IONPs when preventing them from entering the testis, which decreased the ability to nourish the spermatogonia and resulted in a few apoptotic spermatogonia. Notably, although low- and middle-dose administration of IONPs in mice elicited significant sperm quantity and quality decline within seven days (Fig. 4a), extremely limited or no impairment of Sertoli cells has been observed in those mice, suggesting the abnormal sperm parameters elicited by IONPs, to a large extent, were not attributed to the limited Sertoli cells impairment.

Investigation of the Toxicity of IONPs to Epididymis *in vivo*

As mentioned above, the damage to testis or/and epididymides may be potential causes of the abnormal sperm parameters in mice injected with IONPs. Since testis has not been influenced by IONPs obviously, it makes sense to explore whether epididymidis has been impaired after IONPs injection and subsequently caused sperm quantity and quality reduction. Immature sperms from the testis will be transported into the epididymidis to form mature sperms followed by storage during asexual activity. Thus, the significant reduction of sperms in epididymidis of mice injected with IONPs at the first day was probably not correlated with the decreased production of immature sperms or the presence of very few apoptotic cells in the testis. In contrast, we speculated that the reduction of sperm count in epididymidis might be attributed to the direct toxicity of IONPs, as the deterioration of the epididymal environment could also lead to the death of mature sperms. Herein, epididymis index was firstly measured to evaluate epididymal changes. At the first day after injection of IONPs, there were no statistical differences of epididymis index between the control group (mean value, 0.12 %) and even the high-dose IONPs injection group (mean value, 0.10 %) ($P > 0.05$). With the growth of mice, on the 28th day after injection, the epididymis index in all mice increased, but there were still no statistical differences between the control group with each IONPs-injected groups ($P > 0.05$) (Fig. 6a). In addition, we have assessed the weight change of epididymidis and recorded the remarkably similar values between the control group with each administration groups ($P > 0.05$) (Additional file 10: Fig. S10). Moreover, due to the absence of BTB, we speculated that IONPs could directly enter the epididymidis and subsequently accumulated, leading to the death of sperms. This hypothesis was confirmed via the ICP-AES analysis, demonstrated by that the concentration of Fe ions rapidly accumulated in the epididymidis to a maximum value of 44.15 ± 5.20 % ID/g after 1 h, while rapidly dropping to an extremely low level within 24 h (1.99 ± 0.35 % ID/g) (Fig. 6b). The tendency was coincided with the decline and recovery time of sperm count and suggested that the decrease of sperms in the epididymidis was tightly correlated with the accumulation of IONPs, characterized by Fe ions in ICP-AES analysis. In addition to the evaluation of the quantity and quality by analyzing sperms in the suspension, H&E staining was also applied to directly observe sperms in the epididymis. The presence of sperms in the epididymal lumen was hardly observed at the first day after injection with IONPs. As time increased, the number of sperms continued to increase until it returned to the normal range at the 14th day after administration (Fig. 6c). These results were consistent with the parameters revealed by a computer-assisted semen analysis system (Fig. 4a-d). Notably, previous studies have shown that the accumulation of intracellular Fe ions could augment the Fenton reaction to produce a large number of harmful oxidative products [53]. Therefore, oxidative stress may be the underlying

mechanism of sperm death. Malondialdehyde (MDA) is well-known as one of the final products of polyunsaturated fatty acids peroxidation and the increased oxidative stress would cause the accumulation of MDA [54]. However, superoxide dismutase (SOD) is commonly regarded as a natural scavenger of free radicals and main antioxidant enzyme to fight against oxidative stress in the body [55]. To assess the the extent of oxidative stress in epididymidis, the levels of MDA and the activities of SOD were measured (Fig. 6d, e). In the group injected with high-dose (20 mg/mL) IONPs, the MDA level was 18.26 ± 0.57 mmol/mgprot, which was significantly higher than the value of the control group (7.93 ± 0.78 mmol/mgprot) (Fig. 6d). Meanwhile, the SOD activity of 43.05 ± 3.10 U/mgprot in the control group decreased to 26.37 ± 0.82 U/mgprot in the high-dose IONPs injection group (Fig. 6e). These results together suggested that IONPs elevated the oxidative stress in the epididymidis. To further evaluate the damage to epididymidis after IONPs injection, TUNEL staining was utilized to explore the underlying details. As shown in Fig. 6f, a considerable amount of apoptotic cells were observed in the epididymal lumen after the high-dose IONPs administration. The shape and size of apoptotic cells were similar with the abnormal cells indicated by H&E staining of testis, which suggested that the apoptotic cells observed by TUNEL staining may originate from the testis. However, for the epididymal tissues themselves, such as epididymal epithelium, mesenchymal cells, no apoptotic cells were observed. This phenomenon further confirmed that sperms were more sensitive to harmful substances than the other somatic cells. Collectively, we have identified that the elevated oxidative stress levels caused by the accumulation of IONPs in the epididymidis might be one of the underlying mechanisms for the rapid decline of sperm parameters. Given that the sperm damage was temporary and reversible, it may provide some important implications in clinical practice. It is well established that the spermatogenic cycle is critical for continuous sperm production, and the spermatogenic cycle of mice is eight weeks [56]. In consideration of that the reduction of sperm quantity and quality caused by the IONPs injection was able to completely returned to the normal range within two weeks, we speculated that the sperm parameters would be free of abnormalities within a quarter of spermatogenic cycle in male patients who have received MRI examination with IONPs injection, in other words, the fertilized behavior of them was strongly recommended after about 2.5 weeks, which is a quarter of spermatogenic cycle of human beings (10 weeks) [57].

Conclusions

In summary, we have revealed a unique and temporary side effect of IONPs as T_2-MRI contrast agents *in vivo*. Although the systemic toxicities to major organs are negligible after IONPs administration, the male reproductive toxicity should be concerned. The Sertoli cells damage caused by IONPs led to pathological changes and even limited apoptosis of spermatogenic cells in the testis. More importantly, the rapid accumulation of IONPs exerted considerable cytotoxicities to the sperms in the storage organ epididymides, which process might be associated with the elevated oxidative stress. However, the impairment elicited by IONPs was temporary and reversible, by returning to the normal range within 14 days, indicating that the male patients who have received MRI examination with IONPs as contrast agents should carefully delay the fertilized behavior after a quarter of one spermatogenic cycle period.

Collectively, we believe these findings may provide new insights in clinical practice and for better avoiding the side effects that were easy to be negligible with contrast agents administration.

Abbreviations

IONPs: Iron oxide nanoparticles; MRI: Magnetic resonance imaging; RES: Reticuloendothelial system; BTB: Blood testicular barrier; CT: Computerized tomography; T_1/T_2-WI : T_1/T_2-weighted imaging; DWI: Diffusion-weighted imaging; DCEI: Dynamic contrast-enhanced imaging; SPIONs: Superparamagnetic iron oxide nanoparticles; FDA: Food and drug administration; ESIONs: Extremely small iron oxide nanoparticles; MnO NPs: Manganese oxide nanoparticles; GBCAs: Gadolinium-based contrast agents; IONCs: Iron oxide nanoclusters; DMSA: Dimercaptosuccinic acid; ROS: Reactive oxygen species; MDA: malondialdehyde; ZnO NPs: Zinc oxide nanoparticles; PAA: Poly (acrylic acid); ALT: Alanine aminotransferase; AST: Aspartate aminotransferase; Cr: Creatinine; BUN: Blood urea nitrogen; DMSO: dimethyl sulfoxide; ICP-AES: Inductive coupled plasma atomic emission spectrometer; T-SOD: Total superoxide dismutase; SEM: Standard error of mean.

Declarations

Acknowledgements

Not applicable

Authors' contributions

HY Yang and H Wang: Investigation, Conceptualization, Methodology, Data analysis, Formal analysis, Writing-original draft. CH Wen: Data analysis, Formal analysis, Writing-original draft. S Bai: Conceptualization, Methodology, Data analysis. PF Wei: Investigation, Methodology, Data analysis. B Xu: Investigation, Data analysis, Formal analysis. YJ Xu: Investigation, MR Data analysis. CZ Liang: Investigation, Supervision, Resources. YJ Zhang: Investigation, Supervision, Data analysis. GL Zhang: Supervision, Resources, Writing-review & editing. HQ Wen: Conceptualization, Supervision, Resources, Writing-review & editing. L Zhang: Supervision, Resources, Methodology, Data analysis, Formal analysis, Project administration, Writing-review & editing. All authors read and approved the final manuscript.

Funding

This work was supported by National Natural Science Foundation of China (nos. 82072055, 81801831 and 22007006), Key Project of Provincial Natural Science Research Project of Anhui Colleges (no. KJ2019A0278), Supporting Projects for Innovative Leading Talents (no. T000529) and Distinguished Young Scholar of Anhui Colleges (no. gxyqZD2019018), Anhui Provincial Institute of Translational Medicine (nos. 2017ZHYX02 and ZHYX2020A003), Taishan Scholars Construction Engineering (no. tsqn201909144), Special Project of Central Government for Local Science and Technology Development of Shandong Province (no. YDZX20203700001291), the Fundamental Research Funds for the Central

Universities (no. WK9110000062) and Natural Science Foundation of Anhui Province (No. 1808085MB38).

Availability of data and materials

The datasets used and/or analyzed during the current study are available within the manuscript and its supplementary information files.

Ethical approval and consent to participate

All animal experimental protocols and procedures were reviewed and approved by the Institutional Animal Care and Use Committees on Animal Care of Anhui Medical University (Approval No. LLSC20211064).

Consent for publication

All the patients involved in our study obtained written consent for publication.

Competing interests

The authors declare that they have no competing interests.

Author details

[1] Department of Urology, the First Affiliated Hospital of Anhui Medical University, Institute of Urology, Anhui Medical University and Anhui Province Key Laboratory of Genitourinary Diseases, Anhui Medical University, Hefei 230022, China. [2] Reproductive and Genetic Hospital, Department of Radiology, Anhui Provincial Hospital, the First Affiliated Hospital of USTC, Division of Life Sciences and Medicine, University of Science and Technology of China, Hefei 230001, China. [3] School of Pharmacy, the Key Laboratory of Prescription Effect and Clinical Evaluation of State Administration of Traditional Chinese Medicine of China, Binzhou Medical University, Yantai 264003, China. [4] School of Medicine and Institutes for Life Sciences, South China University of Technology, Guangzhou 510006, China. [5] Department of Blood Transfusion, the First Affiliated Hospital of Anhui Medical University, Hefei 230022, China. [6] Center for Scientific Research of the First Affiliated Hospital of Anhui Medical University, Hefei 230022, China. [7] Anhui Provincial Institute of Translational Medicine, Hefei 230032, China.

References

1. Wald LL. Ultimate MRI. J Magn Reson. 2019;306:139-44.
2. Yousaf T, Dervenoulas G, Politis M. Advances in MRI methodology. Int Rev Neurobiol. 2018;141:31-76.
3. Poon C, Gallo J, Joo J, Chang T, Bañobre-López M, Chung EJ. Hybrid, metal oxide-peptide amphiphile micelles for molecular magnetic resonance imaging of atherosclerosis. J Nanobiotechnology. 2018;16:92.

4. Lu Y, Xu YJ, Zhang GB, Ling D, Wang MQ, Zhou Y, et al. Iron oxide nanoclusters for T_1 magnetic resonance imaging of non-human primates. Nat Biomed Eng. 2017;1:637-643.
5. Xu J, Zhang M. Use of magnetic resonance imaging and artificial intelligence in studies of diagnosis of Parkinson's disease. ACS Chem Neurosci. 2019;10:2658-67.
6. Catalino MP, Yao S, Green DL, Laws ER, Golby AJ, Tie Y. Mapping cognitive and emotional networks in neurosurgical patients using resting-state functional magnetic resonance imaging. Neurosurg Focus. 2020;48:E9.
7. Baker JF, Conaghan PG, Gandjbakhch F. Update on magnetic resonance imaging and ultrasound in rheumatoid arthritis. Clin Exp Rheumatol. 2018;36:16-23
8. Litwin MS, Tan HJ. The diagnosis and treatment of prostate cancer: a review. JAMA. 2017;317:2532-42.
9. Shukla G, Alexander GS, Bakas S, Nikam R, Talekar K, Palmer JD, et al. Advanced magnetic resonance imaging in glioblastoma: a review. Chin Clin Oncol. 2017;6:40.
10. Sala E, Rockall A, Rangarajan D, Kubik-Huch RA. The role of dynamic contrast-enhanced and diffusion weighted magnetic resonance imaging in the female pelvis. Eur J Radiol. 2010;76:367-85.
11. Scott LJ. Gadobutrol: a review in contrast-enhanced MRI and MRA. Clin Drug Investig. 2018;38:773-84.
12. Zhao S, Yu X, Qian Y, Chen W, Shen J. Multifunctional magnetic iron oxide nanoparticles: an advanced platform for cancer theranostics. Theranostics. 2020;10:6278-309.
13. Dadfar SM, Camozzi D, Darguzyte M, Roemhild K, Varvarà P, Metselaar J, et al. Size-isolation of superparamagnetic iron oxide nanoparticles improves MRI, MPI and hyperthermia performance. J Nanobiotechnology. 2020;18:22.
14. Briley-Saebo KC, Mani V, Hyafil F, Cornily JC, Fayad ZA. Fractionated feridex and positive contrast: in vivo MR imaging of atherosclerosis. Magn Reson Med. 2008;59:721-30.
15. Lois C, Bezrukov I, Schmidt H, Schwenzer N, Werner MK, Kupferschläger J, et al. Effect of MR contrast agents on quantitative accuracy of PET in combined whole-body PET/MR imaging. Eur J Nucl Med Mol Imaging. 2012;39:1756-66.
16. Reimer P, Balzer T. Ferucarbotran (resovist): a new clinically approved RES-specific contrast agent for contrast-enhanced MRI of the liver: properties clinical development and applications. Eur Radiol. 2003;13:1266-76
17. Chen R, Ling D, Zhao L, Wang S, Liu Y, Bai R, et al. Parallel comparative studies on mouse toxicity of oxide nanoparticle- and gadolinium-based T_1 MRI contrast agents. ACS Nano. 2015;9:12425-35.
18. Weng Q, Hu X, Zheng J, Xia F, Wang N, Liao H, et al. Toxicological risk assessments of iron oxide nanocluster- and gadolinium-based T_1 MRI contrast agents in renal failure rats. ACS Nano. 2019;13:6801-12.
19. Monge-Fuentes V, Garcia MP, Tavares MC, Valois CR, Lima EC, Teixeira DS, et al. Biodistribution and biocompatibility of DMSA-stabilized maghemite magnetic nanoparticles in nonhuman primates

(Cebus spp). Nanomedicine (Lond). 2011;6:1529-44.

20. Garcia-Fernandez J, Turiel D, Bettmer J, Jakubowski N, Panne U, Rivas García L, et al. In vitro and in situ experiments to evaluate the biodistribution and cellular toxicity of ultrasmall iron oxide nanoparticles potentially used as oral iron supplements. Nanotoxicology. 2020;14:388-403.
21. Hong F, Zhao X, Si W, Ze Y, Wang L, Zhou Y, et al. Decreased spermatogenesis led to alterations of testis-specific gene expression in male mice following nano-TiO_2 exposure. J Hazard Mater. 2015;300:718-28.
22. Zhou Q, Yue Z, Li Q, Zhou R, Liu L. Exposure to PbSe nanoparticles and male reproductive damage in a rat model. Environ Sci Technol. 2019;53:13408-16.
23. Zhang X, Yue Z, Zhang H, Liu L, Zhou X. Repeated administrations of Mn_3O_4 nanoparticles cause testis damage and fertility decrease through PPAR-signaling pathway. Nanotoxicology. 2020;14:326-40.
24. Hozyen HF, Khalil H, Ghandour RA, Al-Mokaddem AK, Amer MS, Azouz RA. Nano selenium protects against deltamethrin-induced reproductive toxicity in male rats. Toxicol Appl Pharmacol. 2020;408:115274.
25. Tang Y, Chen B, Hong W, Chen L, Yao L, Zhao Y, et al. ZnO nanoparticles induced male reproductive toxicity based on the effects on the endoplasmic reticulum stress signaling pathway. Int J Nanomedicine. 2019;14:9563-76.
26. Han Z, Yan Q, Ge W, Liu ZG, Gurunathan S, De Felici M, et al. Cytotoxic effects of ZnO nanoparticles on mouse testicular cells. Int J Nanomedicine. 2016;11:5187-203.
27. Mohamed DA, Abdelrahman SA. The possible protective role of zinc oxide nanoparticles (ZnONPs) on testicular and epididymal structure and sperm parameters in nicotine-treated adult rats (a histological and biochemical study). Cell Tissue Res. 2019;375:543-58.
28. Park J, An K, Hwang Y, Park JG, Noh HJ, Kim JY, et al. Ultra-large-scale syntheses of monodisperse nanocrystals. Nat Mater. 2004;3:891-95.
29. Xu YL, Qin Y, Palchoudhury S, Bao YP. Water-soluble iron oxide nanoparticles with high stability and selective surface functionality. Langmuir. 2011;27:8990-7.
30. Arami H, Khandhar A, Liggitt D, Krishnan KM. In vivo delivery pharmacokinetics biodistribution and toxicity of iron oxide nanoparticles. Chem Soc Rev. 2015;44:8576-607.
31. Calatayud MP, Sanz B, Raffa V, Riggio C, Ibarra MR, Goya GF. The effect of surface charge of functionalized Fe_3O_4 nanoparticles on protein adsorption and cell uptake. Biomaterials. 2014;35:6389-399.
32. Di Bona KR, Xu YL, Ramirez PA, DeLaine J, Parker C, Bao YP, et al. Surface charge and dosage dependent potential developmental toxicity and biodistribution of iron oxide nanoparticles in pregnant CD-1 mice. Reprod Toxicol. 2014;50: 36-42.
33. Okam MM, Mandell E, Hevelone N, Wentz R, Ross A, Abel GA, Comparative rates of adverse events with different formulations of intravenous iron. Am J Hematol. 2012;87:E123-4.

34. Hempel JC, Poppelaars F, da Costa MG, Franssen CFM, de Vlaam TPG, Daha MR, et al. Distinct in vitro complement activation by various intravenous iron preparations. Am J Nephrol. 2017;45:49-59.
35. Miao CC, Hu FL, Rui YP, Duan YR, Gu HC. A T_1/T_2 dual functional iron oxide MRI contrast agent with super stability and low hypersensitivity benefited by ultrahigh carboxyl group density. J Mater Chem B. 2019;7:2081-91.
36. Xu YY, Zhou M, Geng HJ, Hao JJ, Ou QQ, Qi SD, et al. Simplified method for synthesis of Fe_3O_4@PAA nanoparticles and its application for the removal of basic dyes. Appl Surf Sci. 2012;258:3897-902.
37. Liu K, Dong L, Xu YJ, Yan X, Li F, Lu Y, et al. Stable gadolinium based nanoscale lyophilized injection for enhanced MR angiography with efficient renal clearance. Biomaterials. 2018;158:74-85.
38. Zelepukin IV, Yaremenko AV, Ivanov IN, Yuryev MV, Cherkasov VR, Deyev SM, et al. Long-term fate of magnetic particles in mice: a comprehensive study. ACS Nano. 2021;15:11341-57.
39. Kievit FM, Stephen ZR, Veiseh O, Arami H, Wang T, Lai VP, et al. Targeting of primary breast cancers and metastases in a transgenic mouse model using rationally designed multifunctional SPIONs. ACS Nano. 2012;6:2591-601.
40. Gómez-Vallejo V, Puigivila M, Plaza-García S, Szczupak B, Piñol R, et al. PEG-copolymer-coated iron oxide nanoparticles that avoid the reticuloendothelial system and act as kidney MRI contrast agents. Nanoscale. 2018;10:14153-64.
41. Ribas-Maynou J, Benet J. Single and double strand sperm DNA damage: different reproductive effects on male fertility. Genes (Basel). 2019;10:105.
42. Bisht S, Faiq M, Tolahunase M, Dada R. Oxidative stress and male infertility. Nat Rev Urol. 2017;14:470-85.
43. Virtanen HE, Jørgensen N, Toppari J. Semen quality in the 21st century. Nat Rev Urol. 2017;14:120-30.
44. Kathrins M. Original descriptions of the relationship between epididymal function and sperm morphology. Fertil Steril. 2017;108:45-6.
45. O'Shaughnessy PJ, Hormonal control of germ cell development and spermatogenesis semin. Cell Dev Biol. 2014;29:55-65.
46. Shiraishi K, Matsuyama H. Gonadotoropin actions on spermatogenesis and hormonal therapies for spermatogenic disorders. Endocr J. 2017;64:123-31.
47. Jiang X, Zhu C, Li X, Sun J, Tian L, Bai W. Cyanidin-3-O-glucoside at low doses protected against 3-Chloro-12-propanediol induced testis injury and improved spermatogenesis in male rats. J Agric Food Chem. 2018;66:12675-84.
48. Teixeira TA, Pariz JR, Dutra RT, Saldiva PH, Costa E, Hallak J. Cut-off values of the johnsen score and copenhagen index as histopathological prognostic factors for postoperative semen quality in selected infertile patients undergoing microsurgical correction of bilateral subclinical varicocele. Transl Androl Urol. 2019;8:346-55.

49. Sofikitis N, Giotitsas N, Tsounapi P, Baltogiannis D, Giannakis D, Pardalidis N. Hormonal regulation of spermatogenesis and spermiogenesis. J Steroid Biochem Mol Biol. 2008;109:323-30.
50. Gerber J, Heinrich J, Brehm R. Blood-testis barrier and Sertoli cell function: lessons from SCCx43KO mice. Reproduction. 2016;151:R15-27.
51. McCabe MJ, Foo CF, Dinger ME, Smooker PM, Stanton PG. Claudin-11 and occludin are major contributors to Sertoli cell tight junction function in vitro. Asian J Androl. 2016;18:620-26.
52. Newton SC, Blaschuk OW, Millette CF. N-cadherin mediates Sertoli cell-spermatogenic cell adhesion. Dev Dyn. 1993;197:1-13.
53. Shen Z, Liu T, Li Y, Lau J, Yang Z, Fan W. Fenton-reaction-acceleratable magnetic nanoparticles for ferroptosis therapy of orthotopic brain tumors. ACS Nano. 2018;12:11355-65.
54. Wang Z, He Z, Emara AM, Gan X, Li H. Effects of malondialdehyde as a byproduct of lipid oxidation on protein oxidation in rabbit meat. Food Chem. 2019;288:405-12.
55. Wang Y, Branicky R, Noe A, Hekimi S. Superoxide dismutases: dual roles in controlling ROS damage and regulating ROS signaling. J Cell Biol. 2018;217:1915-28.
56. Onwuamah CK, Ezechi OC, Herbertson EC, Audu RA, Ujah IA, Odeigah PG. Foetal loss and enhanced fertility observed in mice treated with zidovudine or nevirapine. PLoS One. 2014;9:e107899.
57. Esteves SC, Agarwal A. Novel Concepts in Male Infertility. Int Braz J Urol. 2011;37:5-15.

Figures

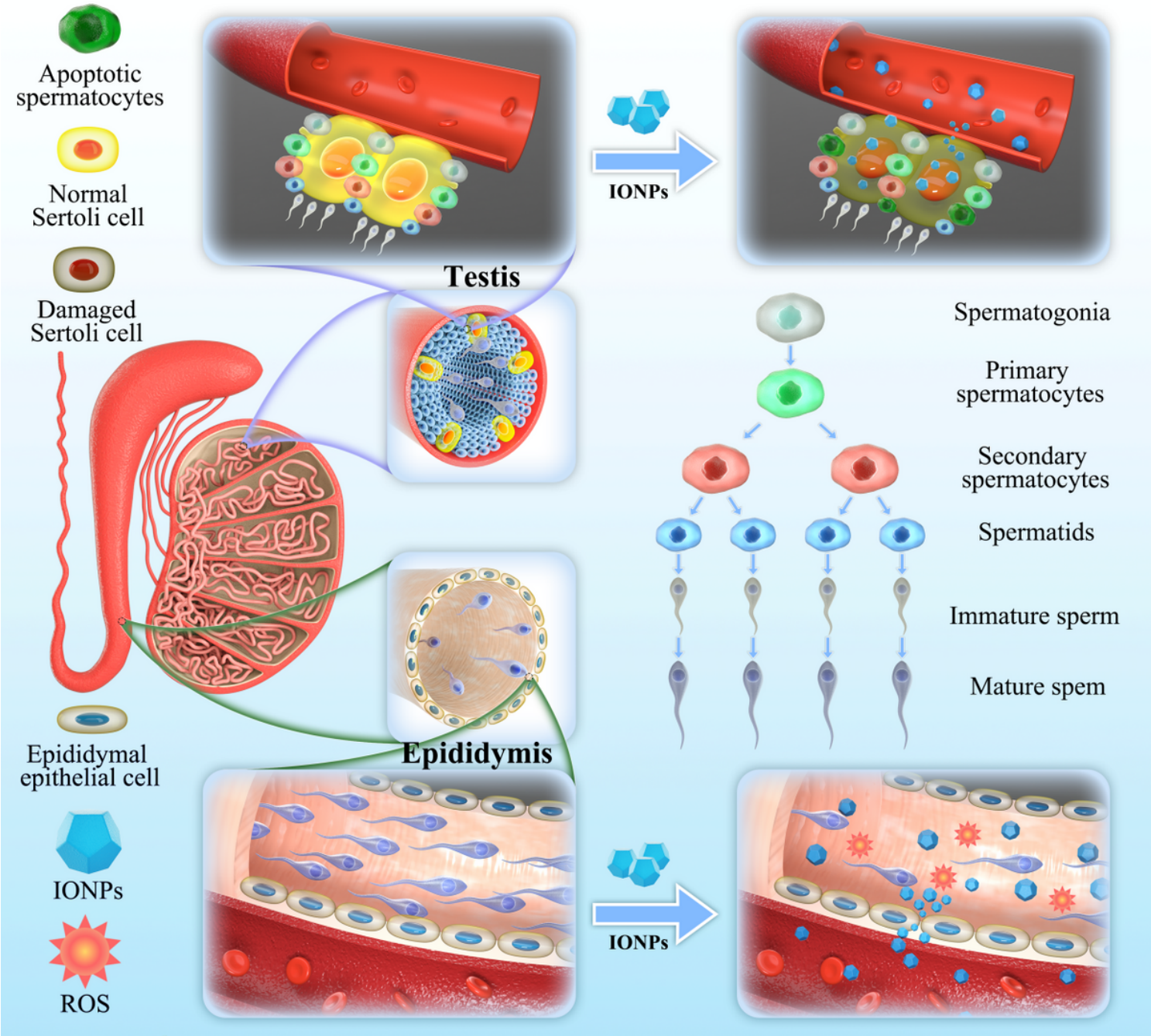

Figure 1

Schematic illustration of effects of intravenously-injected IONPs on testes and epididymides in male ICR mice

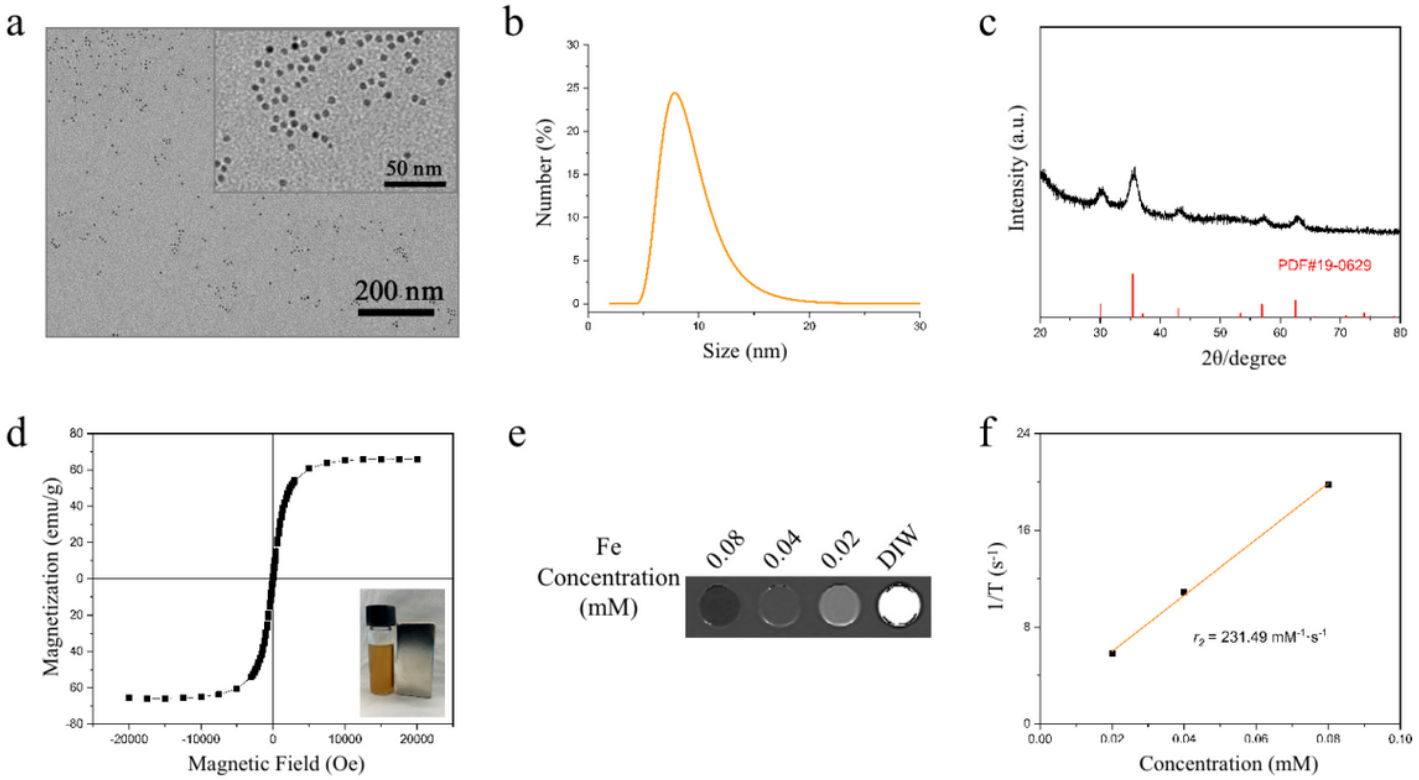

Figure 2

Characterization of IONPs. (a) TEM image and (b) size distribution measured by DLS of IONPs dispersed in aqueous solution. (c) XRD patterns of IONPs. (d) The M-H loop of IONPs at 300 K. Inset showed the response of hydrophilic IONPs to a magnet. (e) T2-weighted image and (f) transverse relaxivity (r2) of IONPs at 3.0 T (R2 = 0.999).

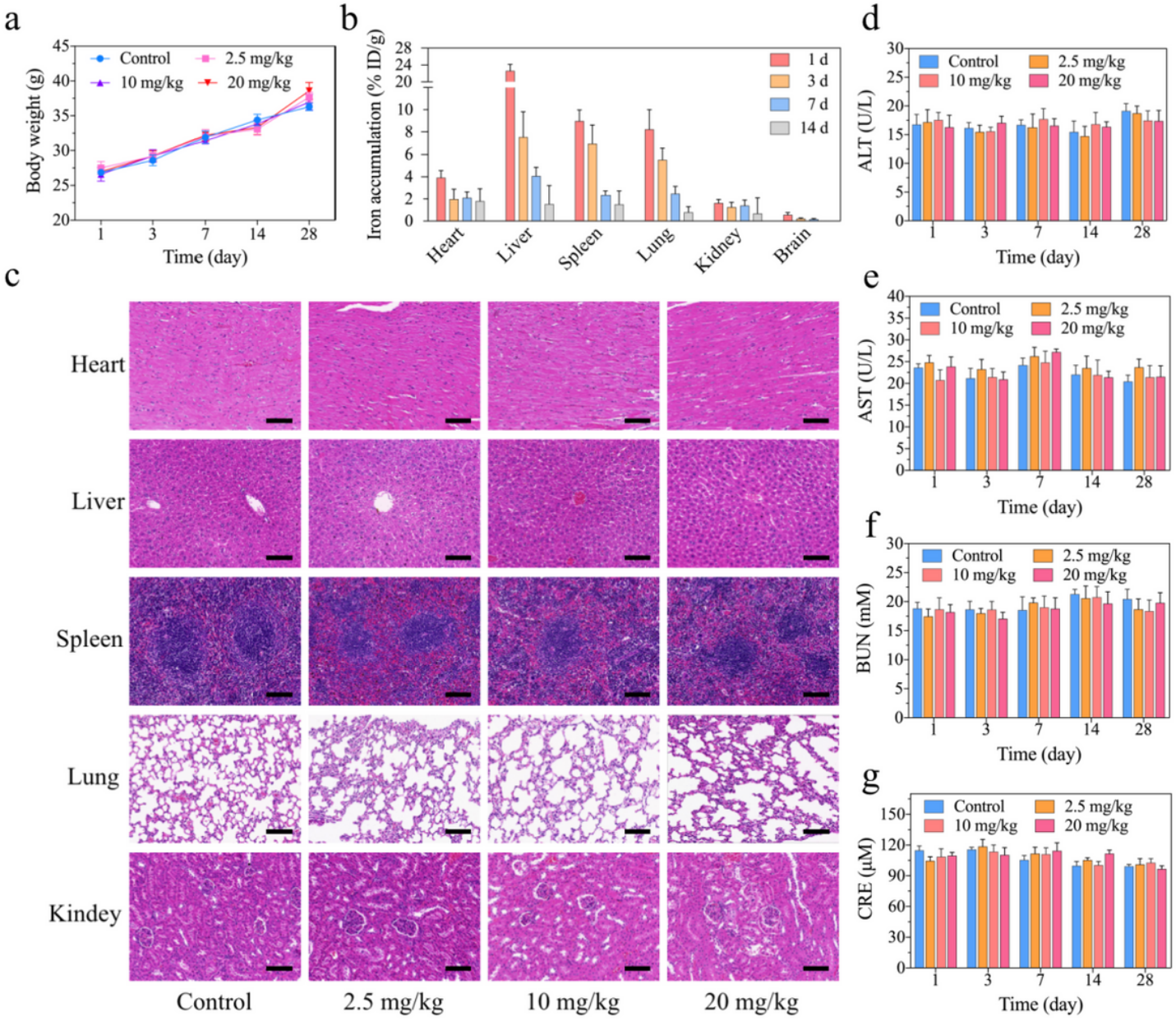

Figure 3

The biocompatibility and distribution of IONPs for major organs in vivo. (a) Body weight curves after intravenous injection of IONPs. (b) The distribution of Fe ions in the major organs of ICR mice at 1, 3, 7, 14 and 28 days after initial IONPs exposure. (c) Histopathological examination of the major organs of ICR mice after intravenous injection of IONPs at various concentrations for 1 day. Scale bar, 100 μm. (d,e) Alanine aminotransferase (ALT) (d) and aspartate aminotransferase (AST) (e) values of ICR mice for assessing liver function after intravenous injection of IONPs at various concentrations for 1 to 4 weeks. (f,g) The parameters of renal function including blood urine nitrogen (BUN) (f) and creatinine (CRE) (g) of ICR mice after intravenous injection of IONPs at three concentrations for 1 to 4 weeks.

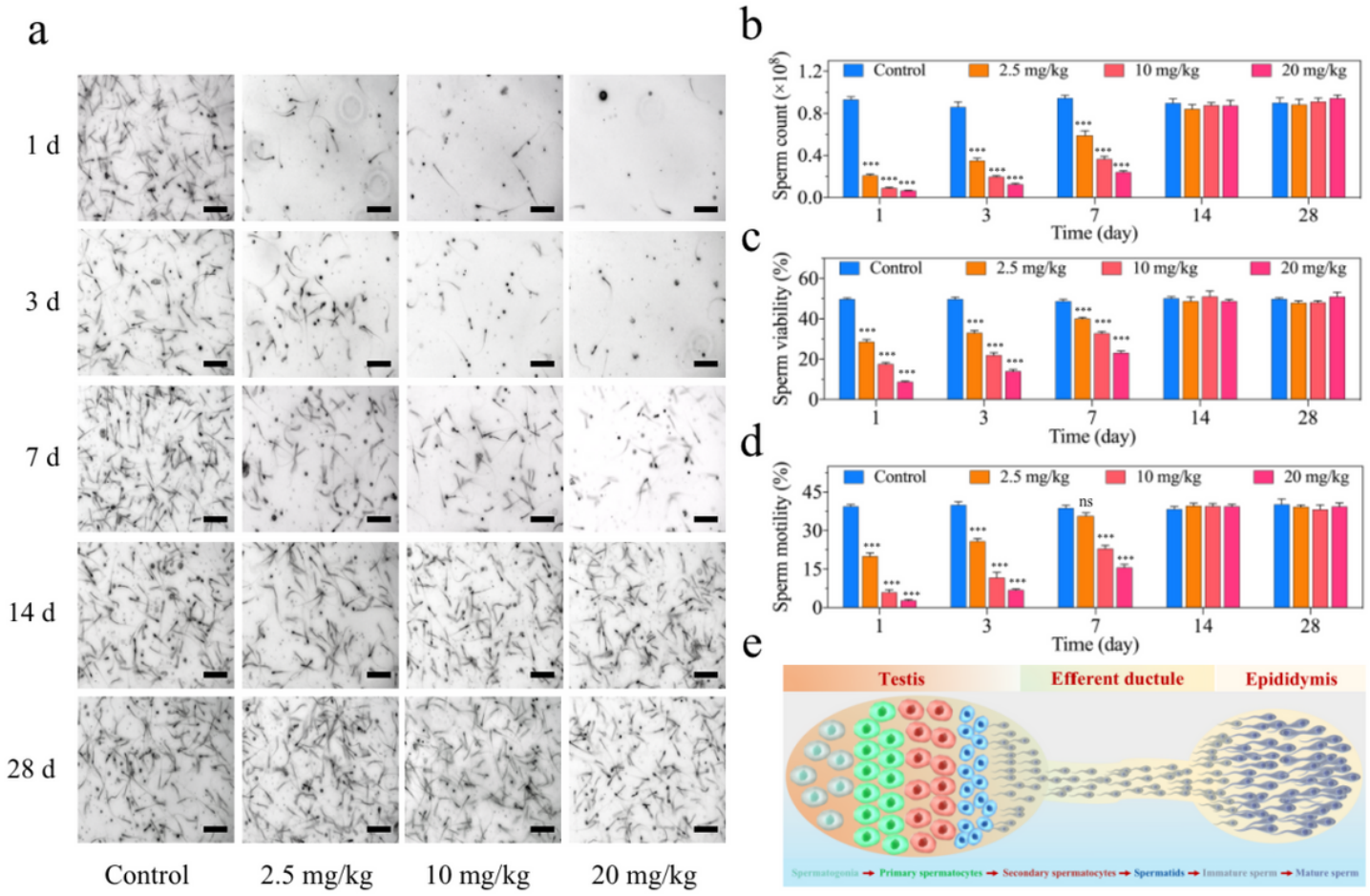

Figure 4

The semen analyses for male ICR mice after IONPs injection. (a) The photos of sperms suspension of ICR mice under microscope at 1, 3, 7, 14 and 28 days after initial IONPs exposure. Scale bar, 100 μm. (b-d) The sperm count (b), motility (c) and viability (d) analyses of ICR mice at 1, 3, 7, 14 and 28 days after intravenous injection of IONPs. (e) Schematic illustration of sperm production, transport and storage. ns, not significant, ***P < 0.001.

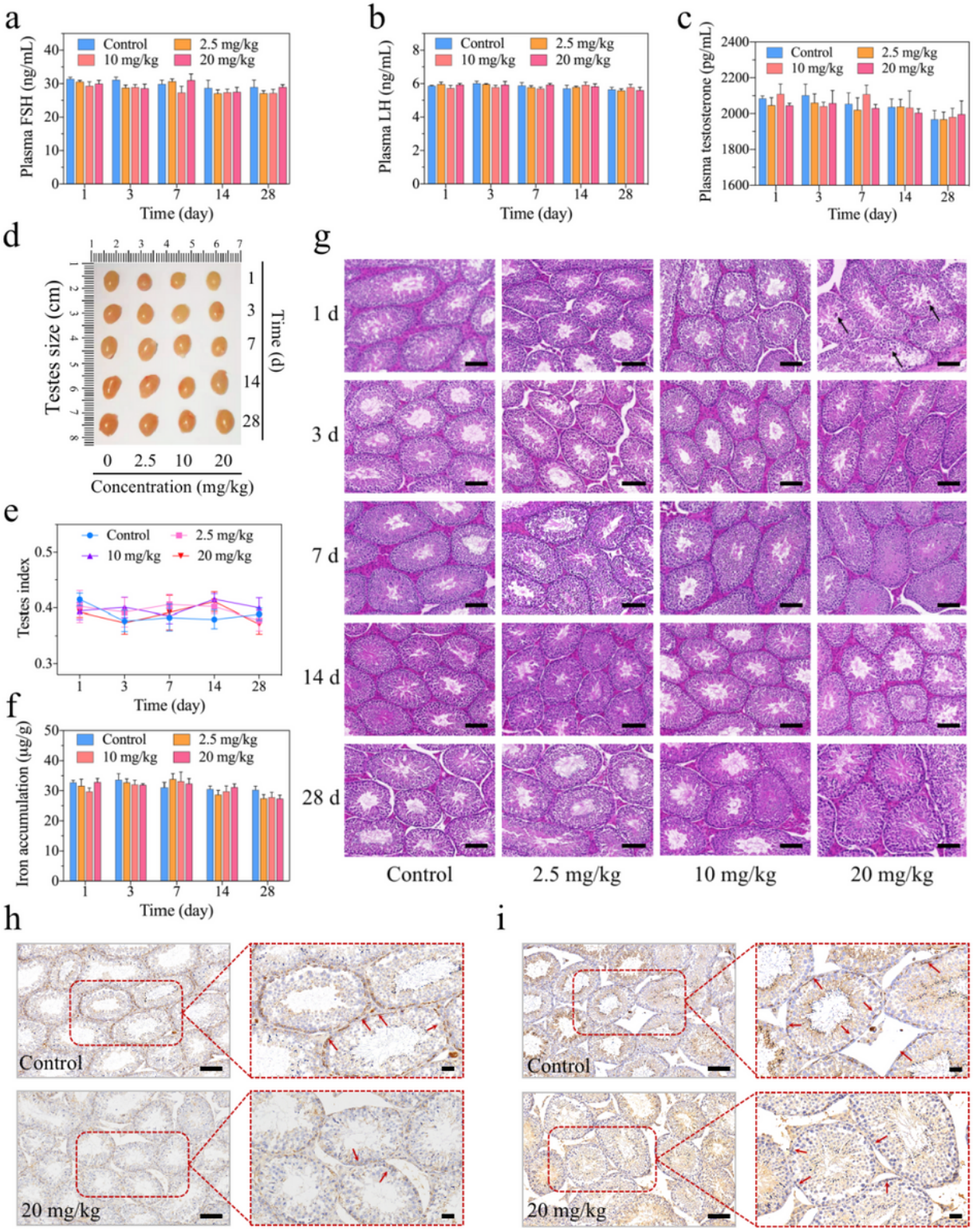

Figure 5

The evaluation of hormones and the effects on testes in male ICR mice with intravenous injection of IONPs. (a-c) The levels of hormones that were highly correlated with spermatogenesis in ICR mice at 1, 3, 7, 14 and 28 days after intravenous injection of IONPs, including FSH (a), LH (b) and testosterone (c). (d-g) The photo of testes (d), testicular index-changing curves (e), accumulation of Fe ions in testis evaluated by ICP-AES (f) and histopathological examination of testes (g) in ICR mice at 1, 3, 7, 14 and 28

days after intravenous injection of IONPs with various concentrations. Abnormal cells were indicated by black arrows. Scale bar, 100 μm. (h,i) Evaluation of N-cadherin (h) and occludin (i) by immunohistological staining. Positive staining was indicated by red arrows. Scale bar, 100 μm.

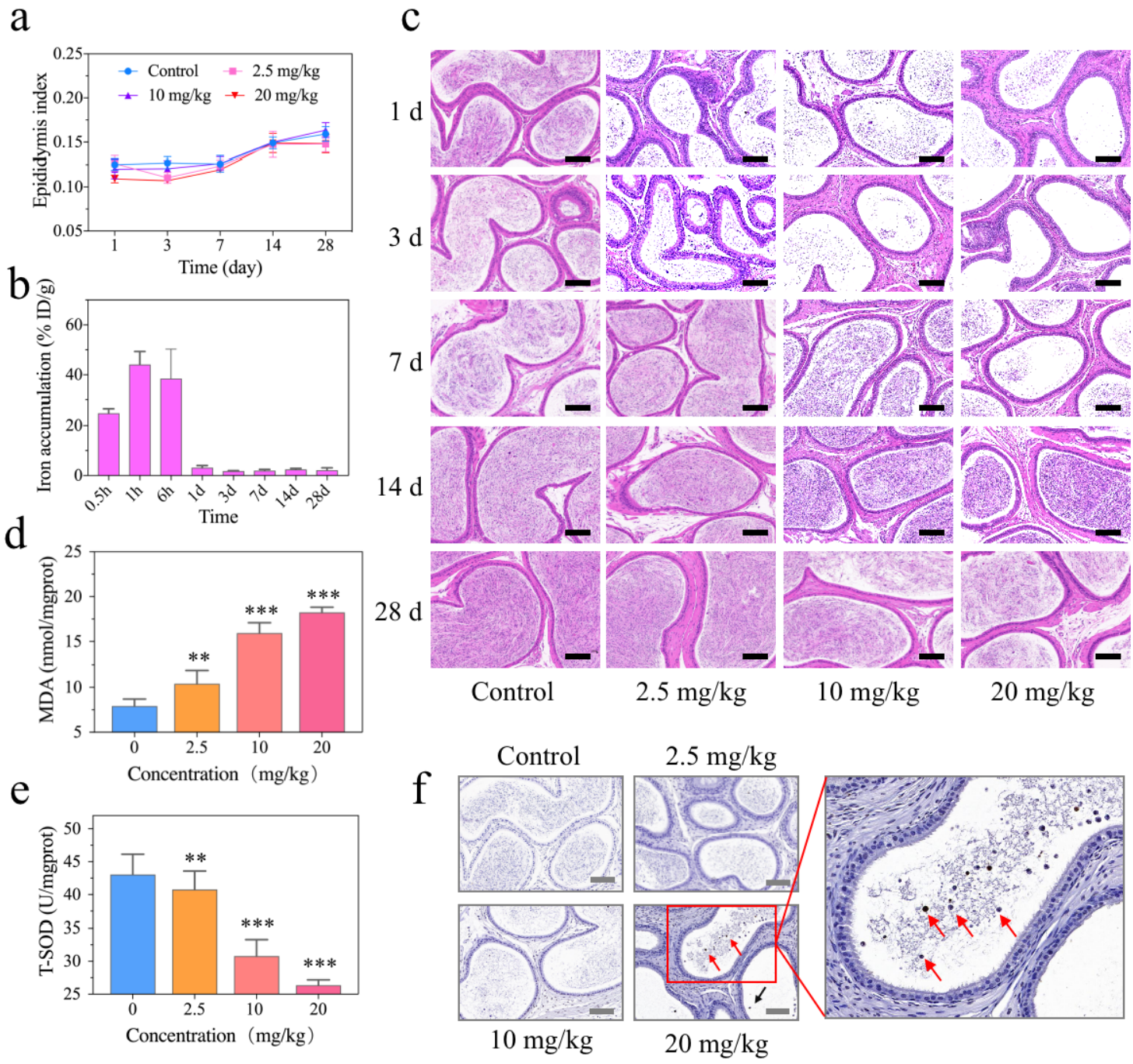

Figure 6

The effects of IONPs on epididymides in male ICR mice. (a-c) Epididymal index-changing curves (a), accumulation of Fe ions in epididymides evaluated by ICP-AES (b) and histopathological examination of epididymides (c) in ICR mice at 1, 3, 7, 14 and 28 days after intravenous injection of IONPs with various concentrations. Scale bar, 100 μm. (d,e) The indexes of oxidative stress in epididymides of ICR mice at 1 day after intravenous injection of IONPs, including MDA (d) and SOD (e). (f) TUNEL staining of

epididymides from sacrificed ICR mice at 1 day after low-, middle- and high-dose IONPs injection. Apoptotic cells were indicated by red arrows. Scale bar, 100 μm. **P <0.01, ***P < 0.001.

Supplementary Files

This is a list of supplementary files associated with this preprint. Click to download.

- Graphicalabstract.png
- SupportingInformation.docx